A Spar Buoy for High-Frequency Wave Measurements and Detection of Wave Breaking in the Open Ocean

ROBIN W. PASCAL, MARGARET J. YELLAND, MERIC A. SROKOSZ, BENGAMIN I. MOAT, EDWARD M. WAUGH, DANIEL H. COMBEN, ALEX G. CANSDALE, AND MARK C. HARTMAN

National Oceanography Centre, Southampton, Southampton, United Kingdom

DAVID G. H. COLES, PING CHANG HSUEH, AND TIMOTHY G. LEIGHTON

Institute of Sound and Vibration Research, University of Southampton, Southampton, United Kingdom

(Manuscript received 30 December 2009, in final form 23 August 2010)

ABSTRACT

Waves and wave breaking play a significant role in the air–sea exchanges of momentum, sea spray aerosols, and trace gases such as CO_2, but few direct measurements of wave breaking have been obtained in the open ocean (far from the coast). This paper describes the development and initial deployments on two research cruises of an autonomous spar buoy that was designed to obtain such open-ocean measurements. The buoy was equipped with capacitance wave wires and accelerometers to measure surface elevation and wave breaking, downward-looking still and video digital cameras to obtain images of the sea surface, and subsurface acoustic and optical sensors to detect bubble clouds from breaking waves. The buoy was free drifting and was designed to collect data autonomously for days at a time before being recovered. Therefore, on the two cruises during which the buoy was deployed, this allowed a variety of sea states to be sampled in mean wind speeds, which ranged from 5 to 18 m s^{-1}.

1. Introduction

There is a growing need for a better understanding of wave breaking and whitecapping in open-ocean conditions (defined here as being far from the coast and usually off the continental shelf). One of the aims of the international Surface Ocean Lower Atmosphere Study (SOLAS) program is to investigate the relationships between wave breaking, whitecap coverage, and air–sea exchanges, or fluxes, of CO_2 and aerosols. Three U.K. SOLAS projects involved direct measurement of these fluxes along with measurements of sea state and wave breaking (Brooks et al. 2009). This paper describes the design and development of a spar buoy at the National Oceanography Centre, Southampton (NOC) in order to obtain high-resolution wave measurements along with images of whitecapping from still and video cameras.

Measuring breaking waves in the open ocean is a challenging task, as noted in the review of wave breaking in deep water by Banner and Peregrine (1993; cf. Melville, 1996). Since that review video footage, conductivity measurements and acoustic sensing have proven to be successful in the study of breaking waves and subsurface bubble clouds in coastal waters (Phelps and Leighton 1998; Gemmrich and Farmer 1999), in the surf zone (Phelps et al. 1997; Deane and Stokes 1999; Leighton et al. 2004), and in lakes (Manasseh et al. 2006). However, there have been few detailed measurements made in deep water in the open ocean (Melville and Matusov 2002; Trevorrow 2003; Gemmrich et al. 2008). To address the continuing dearth of truly open-ocean (i.e., far from the coast) breaking wave measurements, and their relationship to bubble generation and air–sea gas transfer, a new buoy system has been developed at NOC, building on the early work of Longuet-Higgins and Smith (1983, hereafter LHS). The goal was to produce an autonomous buoy that could measure aspects of breaking waves and the associated subsurface bubble clouds for sustained periods, with on-board control and data-logging systems, in the deep water of the Atlantic basin away from the continental shelf.

Corresponding author address: Robin Pascal, European Way, National Oceanography Centre, Southampton, University of Southampton Waterfront Campus, Southampton SO14 3ZH, United Kingdom.
E-mail: rwp@noc.soton.ac.uk

DOI: 10.1175/2010JTECHO764.1

Most wave measurements in the open ocean are made from moored, surface-following buoys, which typically use low sampling rates of either 1 or 2 Hz. Such buoys tend to underestimate crest heights (Forristall 2000), and the resolution of the wave measurements is limited by the size of the buoys, which is generally 1–10 m in diameter. An alternative is to use a spar buoy design, which provides a relatively steady platform from which to make high-frequency wave measurements using capacitive wire wave gauges. To date, few spar buoys have been produced that are capable of operating in the open ocean with deployment periods from days to weeks. For example, LHS used a single wire surface jump meter, but this was not free drifting and was designed to be tethered to either a stationary platform or a ship so that the buoy data could be recorded by external equipment. Similarly, Nelson (1989) used a single wave wire mounted on a lightweight spar buoy for coastal deployments of less than a day. In contrast, the more recent ASIS buoy (Graber et al. 2000) is much larger and is able to operate unattended in the open ocean for a few weeks at a time, either free drifting or moored. The air–sea interaction spar (ASIS) buoy carries an array of eight wave wires that are located within the five support legs of the buoy. The configuration of the wires allows directional wave spectra to be measured, but the upwind support legs may affect the detection of breaking wave events. In addition to the wave wires, the ASIS buoy is designed to carry air–sea interaction equipment (Pedreros et al. 2003). Its design also enables it to withstand high wind speeds but does require very calm conditions to be deployed from a ship.

The NOC spar buoy was designed to be relatively easy to deploy from a ship in calm-to-moderate conditions, but was also robust enough to survive harsh open-ocean conditions. Once deployed, the buoy can be left to drift for up to 1 week so that measurements can be made over a range of conditions. The NOC spar buoy uses a multiple wave wire approach and automatically orientates the wires into the wind so that they are unobstructed. The buoy is also equipped with accelerometers and a compass to measure buoy motion, and downward-looking still and video digital cameras to obtain images of the sea surface. Subsurface bubble clouds were measured using acoustic and optical sensors that were mounted on the buoy by the Institute of Sound and Vibration at Southampton University. This combination of sensors is critical because the detection of breaking waves using wave wires alone is problematic (LHS; see also Banner and Peregrine 1993). The addition of still and video digital cameras allows any wave-breaking detection technique based on the wave wire data to be verified. The low power and small data storage requirements of the wave wire measurements will, in principle, allow much longer records of open-ocean wave-breaking measurements to be obtained in the future, which is the ultimate aim of this part of the project.

The layout of the paper is as follows: the meteorological and sea-state conditions during the initial buoy deployments are described briefly in section 2; section 3 provides a detailed description of the buoy systems; the performance of the buoy is discussed in section 4; and preliminary results are shown in section 5.

2. Field measurements

The NOC spar buoy was deployed during two U.K. SOLAS research cruises on the Royal Research Ship (RRS) *Discovery* in 2006 and 2007. In addition to the standard meteorological and hydrographic equipment found on a research ship, the *Discovery* is equipped with a shipborne wave recorder (SBWR), which measures the 1D wave spectra. An overview of these cruises is given by Brooks et al. (2009), and only a brief summary will be given here.

The NOC buoy was first deployed from the *Discovery* in November 2006 during cruise D313. Owing to exceptionally bad weather the ship was forced to seek shelter among the Western Isles of Scotland for most of the cruise. These sheltered conditions provided a good opportunity for preliminary testing and evaluation of the buoy systems. During D313 the buoy was successfully deployed and recovered from the ship 5 times, although wave data were collected from only three deployments. These three deployments lasted between 1 and 2 h each, during which the maximum 10-min-averaged wind speed recorded by the ship's anemometer reached 18.5 m s^{-1}. Wind speeds used in this paper are all U_{10N}, that is, they have been corrected to a height of 10 m and neutral atmospheric conditions. Because the ship was sheltering, the fetch was short (1–5 Nm) and the maximum significant wave height H_s was only about 2 m.

The second U.K. SOLAS cruise D320 again took place on *Discovery* but this time in the open ocean of the North Atlantic, 400 nm off the coast of Portugal. The buoy was deployed 5 times for periods of up to 3.5 days; longer periods were not possible because of the other activities of the ship. During these deployments wind speeds ranged from 4 to 17 m s^{-1}, with maximum H_s of 5.7 m. Unfortunately, the wave wire system developed an electronic fault only 1 h into the first deployment. This meant that almost no wave wire data were obtained during D320, but the other buoy systems all worked well.

Between the two cruises a number of modifications were made to the buoy, primarily to extend the maximum deployment period. A facility was added to turn the power to the cameras off over night, and a larger–capacity

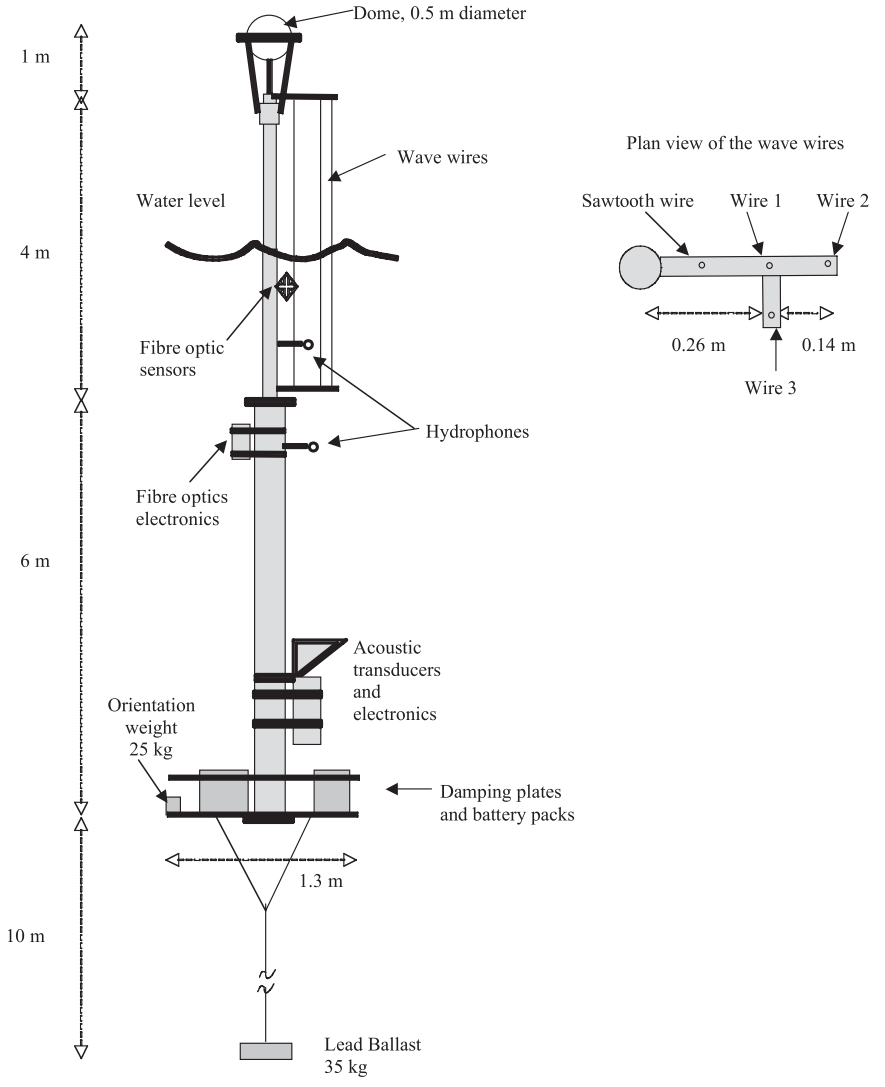

FIG. 1. Schematic of the NOC spar buoy and plan view of the three wave wires (not to scale).

(2 GB) flash card was used for data storage. These modifications extended the maximum deployment duration to 6 days. Other modifications included the addition of a liquid crystal display (LCD) of the logger time to the field of view of the cameras to improve synchronization between systems; the addition of a second stills camera; and an increase in the spacing between the wave wires from 10 to 14 cm. Finally, a method was found by which the buoy could be made to orient itself correctly relative to the wind direction.

3. Spar buoy description

a. Overview

A spar buoy configuration was used to minimize buoy motion and provide a relatively steady platform from which wave elevation measurements could be made by the capacitance wave wires. The main body of the buoy (Fig. 1) consists of two sealed sections of aluminum alloy tubing, with the lower section being 6 m long and 25 cm in diameter, and the upper section being 4 m long and 10 cm in diameter. The wave wires are mounted along the upper section and the buoy is ballasted so that the wires are half submerged, on average. A sealed dome is mounted at the top of the buoy, and this contains the cameras, buoy motion sensors, and electronics for the wave wires. The acoustic and optical systems are distributed along the length of the submerged sections, and have separate electronics housing near the base of the buoy. At the bottom of the spar are two hexagonal damping plates that act to increase the natural period of oscillation of the spar to about 30 s. The buoy has an overall length of 11 m and, including all instrumentation, a total

FIG. 2. A breaking wave passing through the spar buoy.

weight in air of approximately 440 kg. Figure 2 shows the buoy when deployed.

The various systems carried by the buoy have very different power and data storage requirements and were therefore made to be independent of each other (Fig. 3), with each having separate electronics and battery packs. Three battery packs were located between the damping plates—one supplying 24 V, 40 Ah to the optical system, and two others supplying 12 V, 80 Ah to the acoustic system and to the wave wire and camera system. This allowed 6 days of continuous wave wire measurements and 8 h day^{-1} of digital images. Because of power and data storage limitations, the acoustic and optical systems were limited to one continuous 12-h measurement period in each deployment.

The buoy has a number of navigation aids that are housed within the dome at the top of the buoy. These include an Argos beacon, which transmits every 90 s and allows the buoy positions to be e-mailed to the ship every few hours. A ship-installed radio direction finder (RDF) Gonio System provides a bearing on the buoy in real time when the ship is within range. The buoy is also fitted with a Novatech flashing light (RF-700C1) to aid with visibility at night. Each navigation system has an independent power supply, which is sufficient for 3 weeks of continuous operation.

b. Wave and camera systems

The objective of the spar buoy is to make high-temporal-resolution measurements of the wave field and to detect occurrences of wave breaking. Data from buoy motion sensors are used to calculate the low-frequency energy spectrum, and high-frequency surface elevation measurements are obtained from the change in capacitance of the vertical wires. Visual verification of wave breaking is obtained from the digital cameras. All of these systems are housed within an acrylic sphere that sits on top of the buoy. The sphere is split into two hemispheres; the top half is painted bright orange and houses all of the navigation aides, such as the Argos beacon and flashing light. The bottom half is transparent and houses the wave wire electronics, datalogger, buoy motion sensors, and all of the camera systems.

1) DATA LOGGING AND BUOY MOTION SENSORS

Data logging and control of the buoy are performed by a bespoke system developed at the NOC. Output from the wave wire circuits and from a micro-electromechanical system (MEMS) three-axis accelerometer are continuously logged at 41 Hz, and heading, pitch, and roll data from a tilt compensated 3-axis compass module (TCM2.6) are logged at 8 Hz. The accelerometers are used to measure the low-frequency buoy motions that must be combined with the wave wire data to give the true wave motion. They output ± 1.5 g full scale and have a sensitivity of 800 mV g^{-1}.

To calculate buoy motion the horizontal accelerations are converted to pitch-and-roll angles, and combined to produce the buoy tilt. This tilt is then used to correct the vertical axis acceleration, so that a true heave signal is produced. The heave and wire signals are used to calculate separate energy spectra, which are then combined (by simple addition; see section 5a and Fig. 13 below) to produce the full wave spectra.

2) CAMERA SYSTEMS

Two digital cameras, one still and one video, were fitted within the transparent housing at the top of the spar for the first U.K. SOLAS cruise (D313). Both looked straight down at the surface and were positioned so that the wave wires were included in the field of view. Prior to the second cruise (D320), a second stills camera was added to view upwind of the wires in order to detect breaking events, which could be associated with the subsurface bubble clouds.

Power to the cameras is controlled by the datalogger, which disables them at night in order to conserve power and extend the period over which data can be acquired. During D313 and D320 the camera run times were limited by the size of their memory cards (compact flash) and the frequency at which the images are taken; future developments will include cameras with an increased storage capacity. Prior to deployment each camera has its time and date set to coordinated universal time (UTC). Table 1 gives details of the camera systems. During the

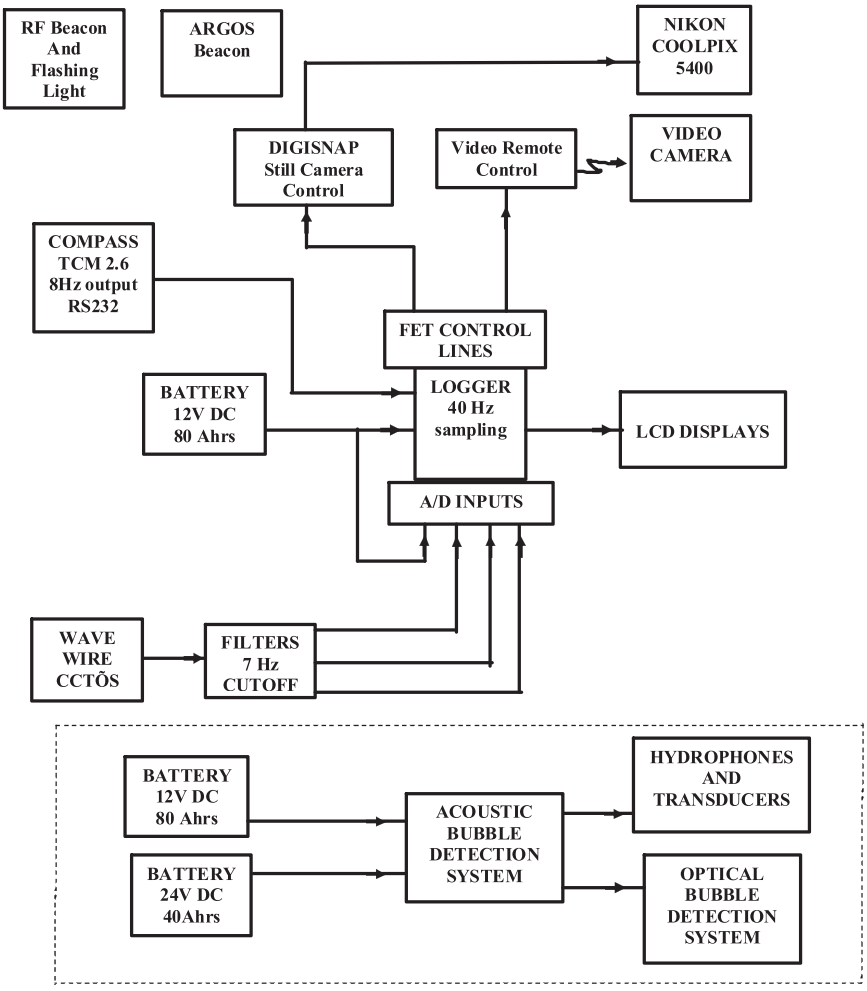

FIG. 3. Block diagram of spar buoy hardware.

longer deployment of D320 the cameras were set to operate during daylight hours only.

To enable the comparison of events seen by the different cameras with the wire data, all of the systems must be synchronized. During D313 the logger time could not be modified while at sea, so offsets to coordinated universal time were noted prior to deployment. In addition, camera images were compared to wire data, with the moment of entry into the water being noted because it was clearly visible in both datasets. After D313 the logger software was modified so that the time and date could be set prior to each deployment. In addition, two LCDs displaying logger minutes and seconds were placed within the field of view of the main still and video cameras. Future developments will include synchronizing all of the systems electronically.

c. Capacitance wave wires

High-frequency wave elevation measurements are made using three capacitance wave wires mounted 14 cm apart horizontally (Fig. 1). The wires are mounted between brackets located 4 m apart vertically. The use of multiple wires allows the surface slope to be estimated. The wave wires are made from polytetrafluoroethylene (PTFE)-coated, multistranded copper wire and are capable of making elevation measurements with a resolution of about ± 3 mm over a 4-m range.

Use of capacitive wire wave recorders for measuring the profile of surface waves is not new (Killen 1952). The sensing element is a partially submerged fine insulated wire, and the capacitance between the wire and the surrounding water varies in a linear fashion. The measured capacitance depends on the amount of wire immersed and also on the thickness of the wire's insulation, which acts as the dielectric of the capacitor. To achieve large capacitive values, long wires with reasonably thin insulation are used. For the NOC spar buoy, a wire of 1.1-mm diameter with a 0.25-mm insulation thickness was used. Each wire was 8 m in length and was mounted folded in two (at 1-cm spacing) around the lower

TABLE 1. Camera details.

Camera	View	Storage	Setup
Video camera (JVC GZ-MG77EK) 2.2 Mp	Narrow field of view (38 mm) downward at wave wires	20-GB hard disk; 37-h continuous	Video 352 × 288 pixels 24 frames per second, 1.5 Mbps
Nikon Coolpix 5400 5 Mp	Wide field of view (28 mm) downward at wires	2-GB CF Approx 22 h	16 images (1.5 Mp each) taken at 2 frames per second every 15 s
Nikon Coolpix 8700 8 Mp	Medium field of view (35 mm) upwind including horizon	4-GB CF Approx 14 h	1 frame (8 Mp) every 10 s

mounting bracket. This doubled the capacitance and removed the need for a robust underwater termination at the bottom of the wire. This arrangement produced a 1.4-nF change in capacitance over the full 4-m range.

The capacitance of the wires is measured using a modified version of G. Novak's femto capacitance meter (online at http://www.nov47.com/cap/cap1.htm), which measures current rather than voltage. The measurement circuit is completely analog so that resolution is only limited by the noise of the system.

A block diagram of the wave wire system can be seen in Fig. 4. A sawtooth waveform is used to generate a constant rate of change in voltage that is applied to one side of the capacitor (the water), enabling a constant current to be measured on the other side (the wire core). The sawtooth waveform can be adjusted so that the produced output covers the range of the 16-bit analog-to-digital converter (ADC) of the logger for the given range of capacitance. For the buoy electronics, the waveform is set to approximately 1.6 kHz, with amplitude of 11 V. This produces an output of 4.8 V for the 1.4-nF full range for the buoy, which compares favorably to the ADC input range of 0–5 V. The current is measured via a current-to-voltage converter, and a peak detector measures the amplitude of the output. The analog output from the peak detector is passed through a 7-Hz, five-pole, Sallen key low-pass filter. The output is then limited in range to protect the ADC inputs by using a rail-to-rail single supply (5 V) unity gain operational amplifier.

For accurate calibration, the wires are removed from the spar and immersed in a bucket of seawater. This allows the immersion depth to be measured accurately, resulting in reliable, reproducible calibrations such as those shown in Fig. 5. These calibrations show a good linear response and very close agreement between the different wires. The variations in the intercept values are due to stray capacitance in the connectors and/or wiring, but such mean biases are removed in the surface elevation calculation. The 1% variation in the slopes shown in Fig. 5 represents the slight variation in the capacitance of individual wires. Also shown is a calibration made in Govan Docks, with the wires mounted on the buoy. The difference between this calibration and that obtained from the laboratory calibration is very small, with a change in slope of less than 0.2%. If wires have to be replaced at sea, bucket calibrations can be made on board the ship in calm conditions (this was not necessary during the actual deployments). It is possible that the wire measurements could be affected by high air fraction and/or spray, but there is no indication in the data acquired during deployments of any unusual responses (e.g., sudden changes in wave elevation and so on, except when breaking appears to be occurring).

d. Subsurface bubble systems

Subsurface bubble populations were measured on the buoy using both acoustic and optical fiber sensors mounted along the length of the buoy. Both sets of equipment shared the same control and data-logging system. A MagnumX 1000 computer running Windows XP and MATLAB controlled the equipment and the data were acquired using a National Instruments PCI-6110multifunction data acquisition (DAQ). The individual systems are described in more detail in the following sections.

1) ACOUSTIC SYSTEM

Acoustic waveforms (Fig. 6) were generated on the computer (with an output sample rate of 1 MHz) and amplified using broadband power amplifiers that were custom made by Blacknor Technology. Three transducers transmitted at frequency ranges of 3–12, 12–30, and 30–200 kHz. The acoustic pulses were received by three D/140 broadband hydrophones located higher up the buoy. To avoid signal loss, the hydrophones were connected to a housing located 1 m away, which contained preamplifiers to condition the signals before transmission to the main housing at the base of the buoy. The signals were then recorded on the DAQ card at 1 MHz.

The acoustic system measured attenuation across a broad range of frequencies, and these attenuation data were then converted into bubble populations (Leighton et al. 2004). A train of 14 pulses was used with a total

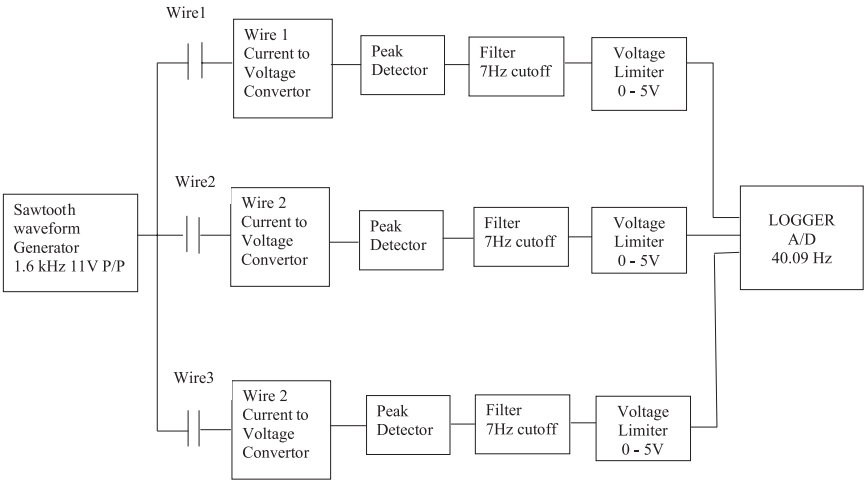

FIG. 4. Block diagram for the wave wire circuits.

duration of approximately 0.2 s. Each pulse was 1 ms long, which was short enough so that the received signal was not affected by surface reflections. A 20-ms gap between pulses prevented energy from previous pulses from interfering with subsequent pulses. The time between pulse trains was approximately 1 s, dictated by the speed at which the computer could save the data files. The pulses varied in frequency from 3 to 197 kHz and measured bubbles from approximately 16 to 1141 μm in radius (the exact values depended in a known way on depth), with the high frequencies measuring small bubbles, and vice versa. Figure 7 shows some of the recorded waveforms from the D320 cruise.

2) OPTICAL FIBER SYSTEM

The fiber-optic system uses the principle that different light intensities will be reflected from the fiber tip depending on whether the tip is in liquid or gas, with the intensity depending on the refractive index of the medium around the tip. As a bubble passes over the tip the change in light intensity can be measured and bubble populations can be inferred using the theory described in Blenkinsopp and Chaplin (2007) and Cartellier and Achard (1991). At the time of writing work is underway to improve upon that original theory.

The system depicted in Fig. 8 can be described in two parts: the optical fiber probes and the optoelectronic amplifier. The fiber probes were built by the Institute of Sound and Vibration Research, with the glass fibers themselves being pulled at the Optoelectronics Research Centre (at the University of Southampton), using the heat-pulling method described by Gates (2004). The tips were conical in shape as recommended by Cartellier (2001). The optoelectronic amplifier was composed of the following four parts: a 5.6-mW light-emitting diode (LED) with a central wavelength of 850 nm, 2 control drivers, a splitter, and 4 light detectors. The splitter divides the light from the LED into 4 separate channels, and 4 silicon photodiode detectors are used to transform the light intensity into currents. Transimpedance amplifiers convert the currents into voltages, which are recorded with a sample rate of 100 kHz.

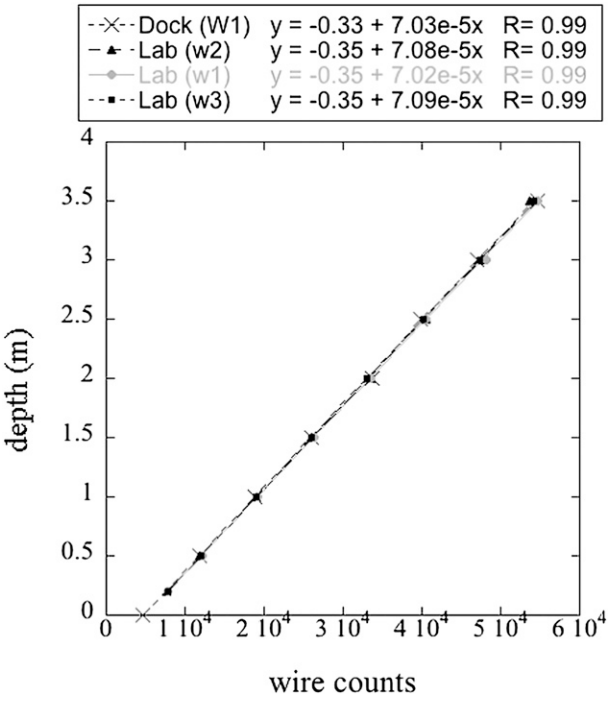

FIG. 5. Laboratory calibration of 3 spar buoy wave wires. Wire 1 (black triangles), wire 2 (gray circles), wire 3 (black square), and D313 wire 1 (black crosses) from the calibration in Govan Dock.

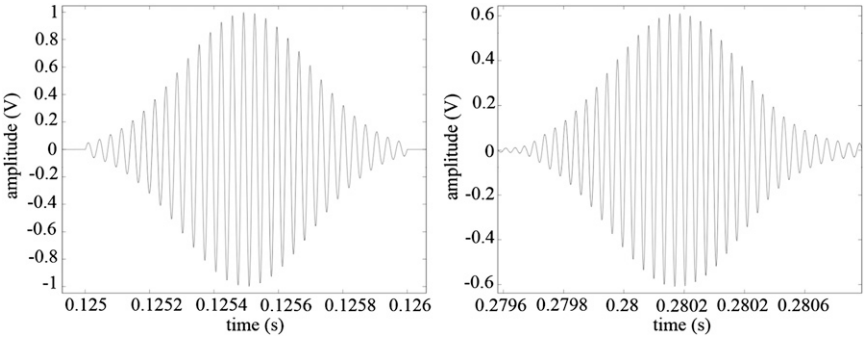

FIG. 6. The transmitted 29-kHz signal from (left) the signal generator and (right) the same pulse as received at the hydrophone demonstrating the high fidelity of the source. Note change of scale in the *y* axes.

4. Spar buoy performance

This section examines the performance of the buoy in terms of its stability and robustness. The orientation of the wave wires with regard to the wind direction is also discussed.

a. Buoyancy and stability

The 6-m-long lower section of the spar displaces 314 kg of water and the immersed half of the upper section displaces 26 kg of water. An additional 100 kg of displacement is provided by the electronic housings and battery packs. The total mass of the buoy, including instrumentation and suspended ballast weight, is 440 kg. This gives a natural period of oscillation of about 20 s. The buoy design includes a damping plate to improve buoy motion, which increases the natural period to around 30 s. Figure 9 shows the wire depth immediately after deployment into calm freshwater. The buoy's natural period of oscillations can clearly be seen.

The mean tilt angles of the buoy to the vertical, and its variation about the mean angle, were examined using data from the three-axis compass unit. During the second deployment of cruise D320, the compass failed so that tilt angles were calculated from the accelerometer data that had previously been calibrated against the compass data. Figure 10 shows typical mean tilt angles calculated over 10-min periods and plotted against wind speed. Typical mean tilts ranged from 2° to 14° for winds between 5 and 18 m s^{-1}. Standard deviations were generally small, with the largest pitch-or-roll standard deviations being 3.3°–5.6° over the same wind range.

During cruise D313 the buoy was deployed in sheltered coastal conditions with very little swell (maximum H_s of around 2 m) but high wind speeds (with a maximum 10-min average of 18 m s^{-1}). However, the tilts

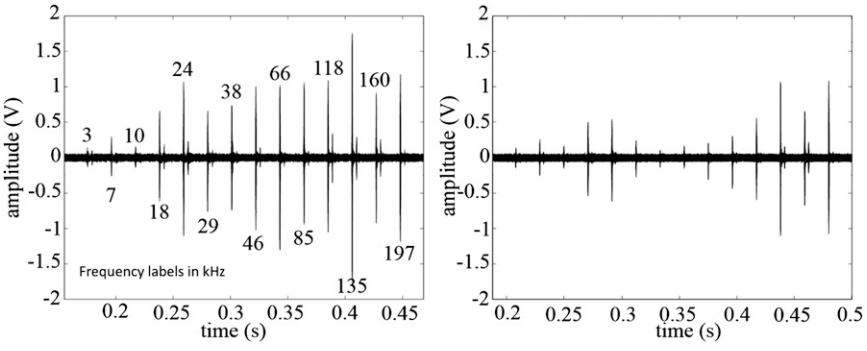

FIG. 7. (left) A train of pulses as recorded on one of the hydrophones when very few bubbles were present. Each pulse is labeled with its frequency (kHz). (right) A train of attenuated pulses recorded in the presences of bubbles. The time scale means that the sinusoidal oscillations within each pulse are not visible. This pulse train was repeated approximately once per second.

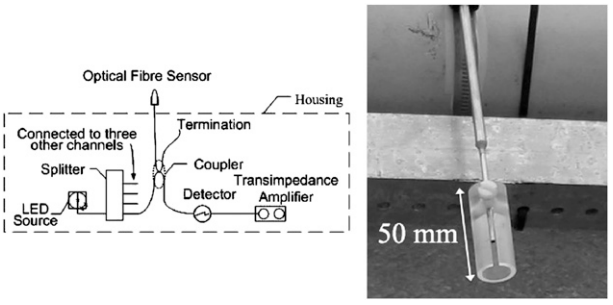

FIG. 8. (left) A schematic showing the optical fiber system. (right) The optical fiber sensor with protective plastic cap (slid back for deployments). The actual fiber protrudes approximately 10 mm out of the metal casing.

during deployments 4 and 5 (when the wind speeds were high) for D313 were much larger than those during D320. This was due to the use of a partly submerged vane on the buoy that was intended to orientate the wires in to the wind (see section 4.b below). The vane failed to do this and instead acted to greatly increase the windage of the buoy, which responded by tilting away from the vertical. The vane was removed prior to cruise D320.

During cruise D320 the buoy was deployed in full open-ocean conditions with much larger swells. The largest waves were encountered during the second deployment of D320, which had a maximum wind speed of 14.1 m s^{-1} and H_s of 5.7 m, with individual peak-to-trough heights of up to 9 m. Despite this the mean tilt of the buoy was only about 5°.

During this second deployment the fiber optics electronics housing flooded, which resulted in the buoy being submerged 0.25 m lower in the water. The mean tilts during this period were a little lower than may be expected, possibly resulting from the reduction in windage caused by the buoy being lower in the water. Figure 11 shows H_s estimates from the SBWR and from the buoy during the storm. The H_s from the buoy was calculated from the motion sensors only because the wave wires did not work; hence, buoy H_s is underestimated (see section 5). During the last 18 h of day 181 the SBWR H_s estimates varied from 4 to 6 m; in this time there were three or four occasions when the buoy may have been completely submerged very briefly. These events are shown by unrealistically large H_s values from the buoy. Few of the submersion events were associated with the largest SBWR H_s values or with the largest peak-to-trough waves, which suggests that the buoy is responding reasonably well even to the largest waves, in the sense that it was riding these well without becoming submerged and returning reliable estimates of H_s. However, a wave breaking on top of the

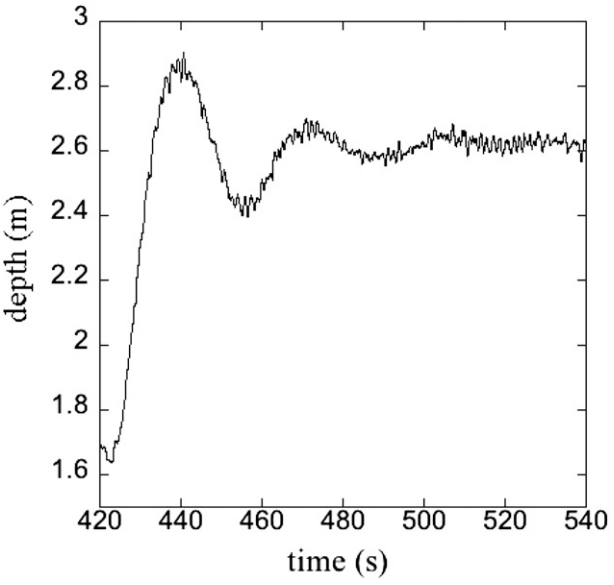

FIG. 9. The natural period of oscillation of the buoy.

buoy and submerging it or knocking it down would cause the buoy to oscillate until it had regained equilibrium. These oscillations and large accelerations would cause the spuriously large H_s values seen in Fig. 11. There is evidence from the camera data that the submersion events were indeed due to waves breaking across the top of the buoy. The reduced buoyancy resulting from the

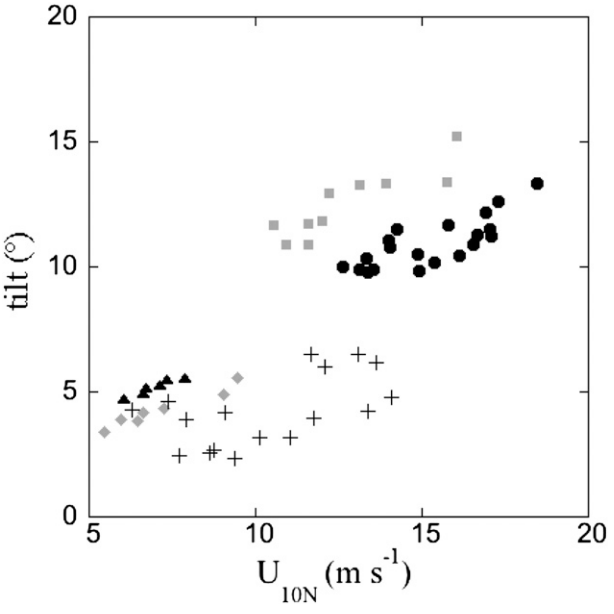

FIG. 10. Buoy tilt angles: D313 deployment 2 (gray diamonds); D313 deployment 4 (black circles); D313 deployment 5 (gray squares); D320 deployment 1 (black triangles), and D320 deployment 2 (crosses).

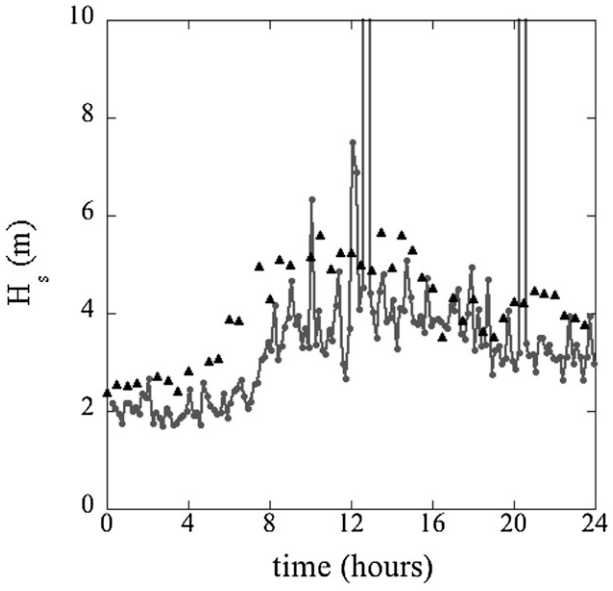

FIG. 11. Significant wave height estimates H_s (m) from the SBWR (black triangles) and the spar buoy motion sensors (gray) are shown for day 181, the peak of the storm for deployment 2 of D320. The effects of submersion events can be seen in the H_s from the spar buoy.

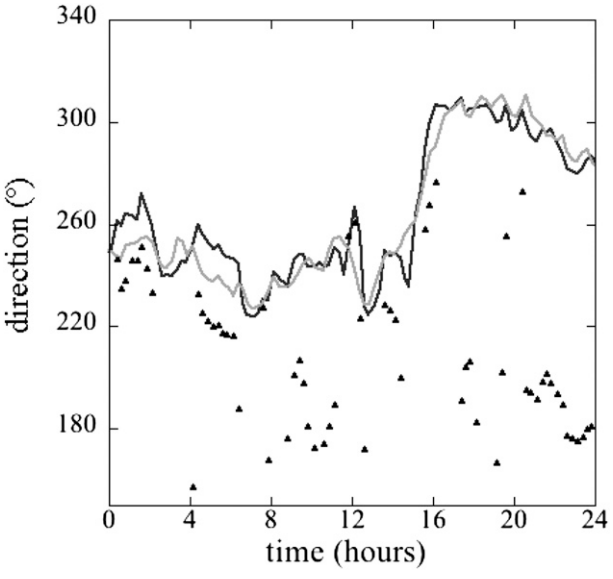

FIG. 12. The 15-min averages of buoy heading (gray line), true wind direction from ship measurements (black line), and wind direction relative to the ship (triangles).

flooded electronics housing makes these submersion events more likely. It is not known if, had the flooding not occurred, the normal behavior of the buoy would have prevented submersion events.

b. Orientation

The buoy should be oriented so that the wave wires and acoustic and optical systems are upwind of the spar body to ensure that the body does not interfere with the wave action and bubble clouds before they are measured. During D313 a partially submerged vane was mounted along the top section of the buoy, so that the buoy would orient relative to the wind and currents. The vane was kept relatively small so as not to alter the dynamic response of the buoy unfavorably. However, this proved to be unsuccessful and subsequent trials showed that, when tilted, the buoy rotated about its center of mass and that the vane was far too small to prevent this. Fortunately this rotation could be used to control the buoy orientation as desired. A 25-kg weight was mounted on the damping plate on the opposite side of the spar to the wave and bubble systems. Any wind-induced tilt of the buoy caused it to rotate to bring the weight to the lowest point, thus bringing the wires and bubbles to the upwind side of the spar.

This method worked very well, achieving excellent exposure for the wires and bubble systems. This orientation to wind was so reliable that the buoy heading, as measured by the onboard compass, gave a good estimate of the wind direction. Figure 12 compares 15-min averages of buoy heading with true wind direction as measured on the ship for one 24-h period. During this period the wind speed remained fairly constant with a mean of 7 m s^{-1} (std dev 1 m s^{-1}), but the true wind direction changed from 240° to 300° over a 2-h period. The buoy heading tracks the wind direction very well, with a mean offset for the period of less than 2° (std dev 8°).

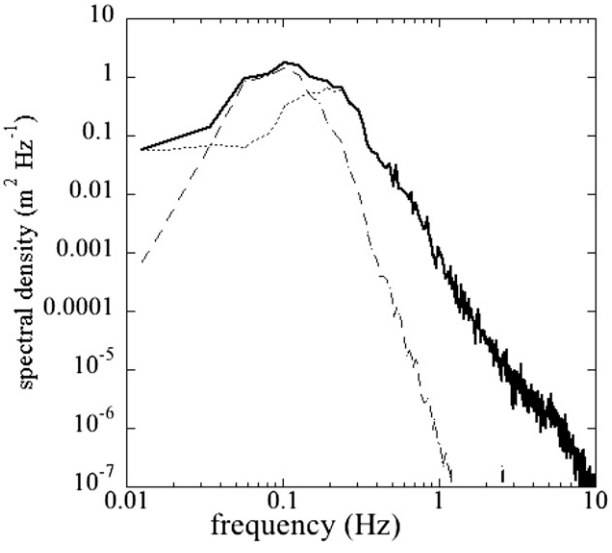

FIG. 13. Wave spectra from D313 deployment 5. Heave spectrum (dashed), wire spectrum (dotted), and the combined spectrum (solid).

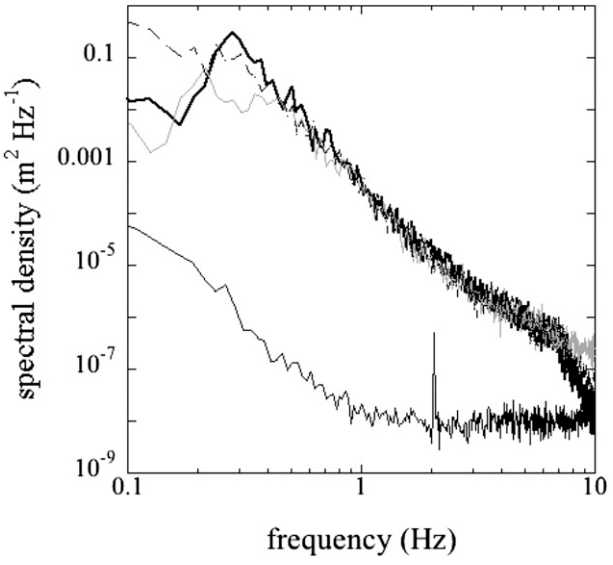

FIG. 14. Wave wire spectra (no heave component) from D313 obtained for a range of wind speeds: 6.4 (gray), 11.6 (dashed), and 17.2 (thick black) m s^{-1}. Also shown is a 0 test (thin black). Note that the low-frequency (<0.1 Hz) parts of the spectra are not shown.

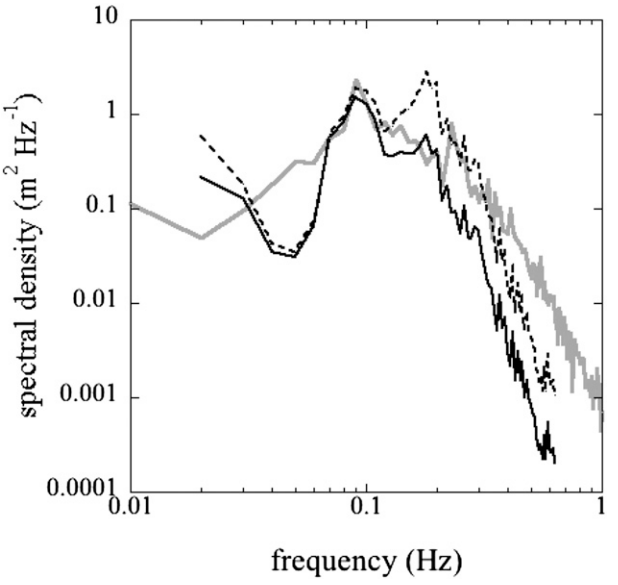

FIG. 15. Wave spectra from the spar buoy (gray), the SBWR (black), and the SBWR with a correction for ship response (dotted).

The agreement between the buoy heading and wind direction is best when the wind is blowing onto the bow of the ship (with a relative wind direction of 180°). The agreement becomes less good as the wind moves away from the bow, because the airflow distortion over the ship deflects the wind in the horizontal plane (Yelland et al. 2002).

Although the buoy orientates well into the wind it is possible that the wind and waves may not be aligned, and this might affect the detection of wave breaking. In principle, the data from the wave wires and the pitch-and-roll sensors on the buoy could be used to make some estimate of wave directionality, but this remains to be investigated. The wave wires are rather closely spaced (14 cm) to obtain much in the way of meaningful wave directionality information, except perhaps for very short wavelength waves. In contrast, the pitch-and-roll sensors will pick up motion from longer-scale waves, but the buoy has been designed to minimize its response to such waves, so it is unclear again whether meaningful information on wave directionality can be obtained.

5. System performance and initial results

a. Wave spectra

As noted in section 2, the wave wire electronics failed early on in cruise D320, so the data used to examine the wires' performance is limited to that obtained during cruise D313.

The buoy heave spectrum, calculated from the three-axis accelerometer and the wave wire elevation spectrum, are combined to produce the full wave spectrum for each 10-min segment of data. The moments of the combined spectra are used to calculate parameters, such as significant wave height H_s and zero up-crossing period T_z. Figure 13 shows a combined wave spectrum from

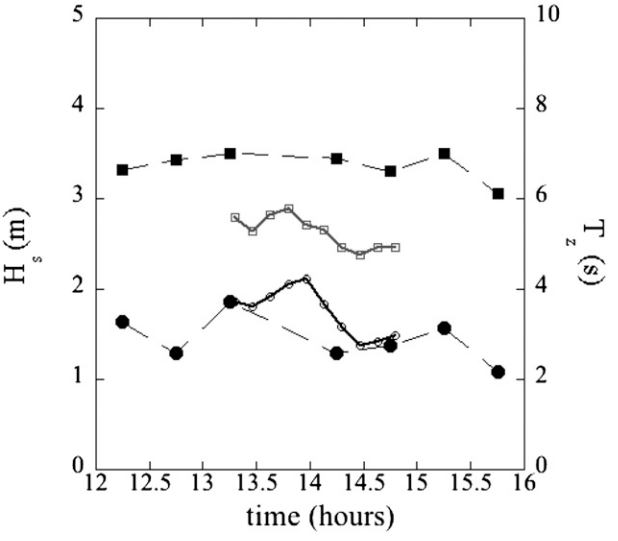

FIG. 16. The D313 deployment 5: SBWR H_s (black solid circles), buoy H_s (black line with open circles), SBWR T_z (black solid squares), and buoy T_z (gray line with open squares). Buoy data were processed with spectra truncated at 0.63 Hz. During the 2 h that the buoy was deployed wind speed increased from 10 to 15 m s^{-1}, and then decreased back to 10 m s^{-1}.

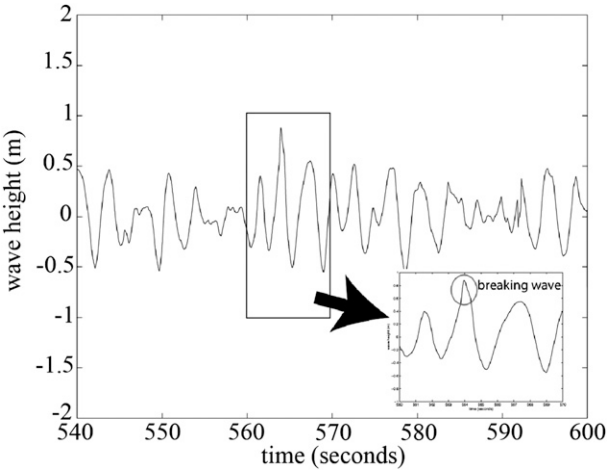

FIG. 17. A 1-min example of a wave trace. The inset panel to the right of the arrowhead shows a breaking wave.

D313 deployment 5 along with the individual heave and wave wire spectra. As expected, the heave spectrum makes a significant contribution at low frequencies. This contribution would be much larger for D320 when swell was present.

To give an indication of the noise levels in the system, Fig. 14 shows typical wave wire spectra (no heave component) for a range of wind speeds along with a still water laboratory spectrum. This shows that the noise spectrum is at least an order of magnitude below the wave spectra up to and beyond the filter cutoff at 7 Hz. The spike at 2 Hz in the laboratory spectrum is probably due to electrical noise from other laboratory equipment. The spectra obtained at a wind of 6 m s^{-1} show an in increase in noise above 7 Hz due to a broken wire in the electronics which occurred during that deployment.

b. Comparison to shipborne wave recorder

To give a first-order check of the spar buoy measurements, buoy data were compared to those from the SBWR mounted on RRS *Discovery* during the same period. The SBWR was devised by Tucker (1956) and developed further at the Institute of Oceanographic Sciences, Wormley (later to become part of NOC). The SBWR has been used extensively for many years for offshore wave measurement in the northeast Atlantic, on light vessels and weather ships (Bacon and Carter 1991), and is still used on some research ships today (Holliday et al. 2006; Yelland et al. 2009).

Figure 15 shows wave spectra from the spar buoy and from the SBWR: the latter are limited to 0.625 Hz. Reasonable agreement is seen for frequencies below 0.2 Hz. Above 0.2 Hz the SBWR spectra tend to underestimate the energy because the size of the ship limits its response to the shorter wavelengths. An instrument and ship correction based on ship length and sensor depth (Pitt 1991) can be applied to the SBWR spectra. The corrected spectrum is also shown in Fig. 15. This improves the spectrum to some degree for the higher frequencies but overcorrects in the region around 0.3 Hz. This leads the corrected H_s data to be biased high, so the SBWR H_s used hereon are from uncorrected spectra. The correction has a larger effect on T_z, with the uncorrected data being biased toward the longer period waves. Both buoy and (uncorrected) SBWR H_s and T_z data from D313 deployment 5 are shown in Fig. 16. In this case the buoy spectra were truncated to 0.63 Hz, before calculating H_s and T_z, in order to make a direct comparison with the SBWR data. The SBWR makes no allowance for ship speed through the water, so data obtained while the ship was steaming have been removed. Figure 16 demonstrates good agreement in H_s and the low-frequency bias in T_z of the SBWR. In contrast, Fig. 11 showed H_s from both systems during a storm encountered during D320 where, because there are no wire data, the buoy tends to underestimate H_s by about 1 m.

c. Wave-breaking detection

The wave wire data from D313 were analyzed for the detection of breaking waves using the method described by LHS. They used the theory that a gravity wave can have a maximum inclination of 30.4° (Longuet-Higgins and Fox 1978), and so a breaking wave can be detected by a jump in surface elevation, which corresponds to an inclination of more than 30°. LHS used a single wave wire so the surface inclination was calculated via the time derivative of the surface elevation. For each wire of the NOC spar buoy, the time derivative of the surface elevation was divided by the phase speed of the wave to give the surface inclination or ''temporal slope.'' The phase speed c_p was calculated from the mean T_z value for each 10-min section of data (following LHS), using

$$c_p = \frac{gT_Z}{2\pi},$$

where g is acceleration resulting from gravity. The possible problems with using c_p derived from T_z are discussed below.

Because the NOC spar buoy has three wires it is also possible to calculate the surface inclination directly using the difference in surface elevation from pairs of wires. This we term the ''spatial slope.''

Data from D313 deployment 4 were analyzed using the assumption that wave slopes exceeding the 30° threshold indicate waves that are breaking or just about

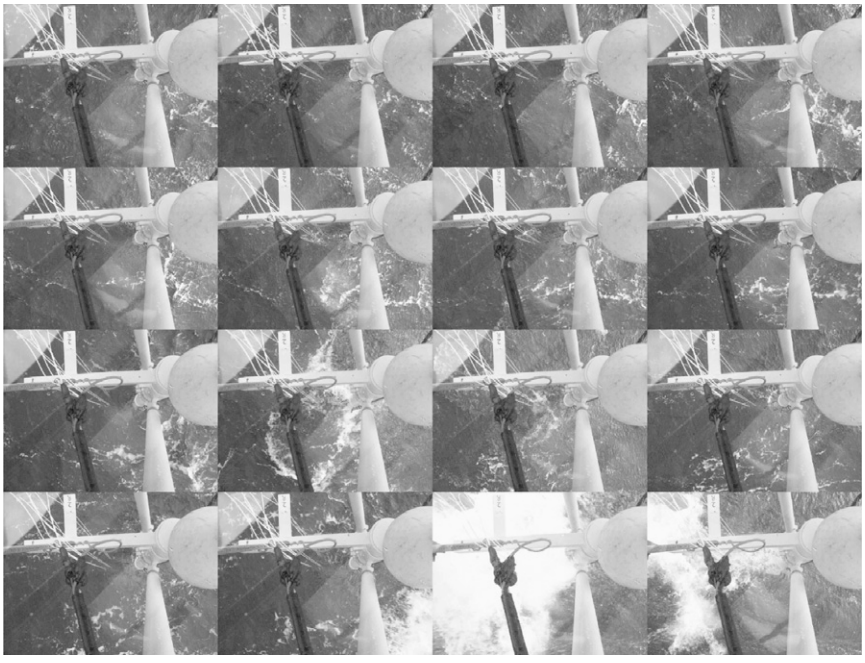

FIG. 18. Images from the stills camera showing the breaking wave identified in Fig. 17. The sequence is left-to-right and the images are 0.5 s apart.

to break. The results were compared with video footage over the same period. The video footage is analyzed manually ''by eye'' and, because this is rather labor intensive, only 45% of the twenty 10-min sections available have been analyzed. The problem of orienting the wires into the wind had not been solved during D313, and it was found that occasionally one of the wires would be sheltered by the body of the buoy. Because of this, data from all three wires were analyzed and the average of the largest two slopes was used in the threshold detection. A typical wave trace from a single wire can be seen in Fig. 17 and digital camera images for the same period can be seen in Fig. 18. A breaking wave can be clearly seen in both.

Using the 30° threshold, the number of breaking waves in each 10-min section of data was counted. The results are shown in Figs. 19 and 20 for the temporal and spatial slopes, respectively. Also shown are the number of breaking waves seen in the video footage, and the mean wind speed for each section. The number of events detected in the video data follows the trend in the mean wind speed very well, with the number of breaking waves increasing from 10 to 15 as the wind increased from 12 to 18 m s^{-1}. However, it can also be seen that the number of breaking waves as derived from the temporal and spatial slopes are very much underestimated compared to the video data, as has been noted before (Banner and Peregrine 1993; see their Fig. 2 reproduced from Holthuijsen and Herbers 1986). This reflects the different criteria being used to detect breaking. Here, for simplicity, the slope threshold was reduced until reasonable agreement was found between the wire and video results. This was obtained with thresholds of 24° and 17° for the spatial and temporal slopes, respectively. Although mean agreement was achieved by lowering the threshold angle, close inspection of the timing of the events showed that a significant fraction of those detected by the wires did not correspond to those seen in the video data. Only 43% of temporal slope events and 31% of spatial slope events occurred at the same time as the events seen in the video footage. This may be partly due to the criterion that is used to determine the phase speed, in that the average phase speed over the measurement period of 10 min will almost certainly not be the phase speed that would be determined from the actual wave period associated with each individual breaking event. The phase speed determined from T_z will be representative of the longer waves, while the breaking may be occurring on smaller wave scales.

The wave wire data are the subject of ongoing analysis. To improve the wave-breaking detection capabilities of the new buoy alternative criteria are being developed to detect wave breaking based on the wave wire data. These include using various measures of the variance of the surface elevation and slopes over short segments of the observations (typically a few tenths of a second). The results of one such example are shown in

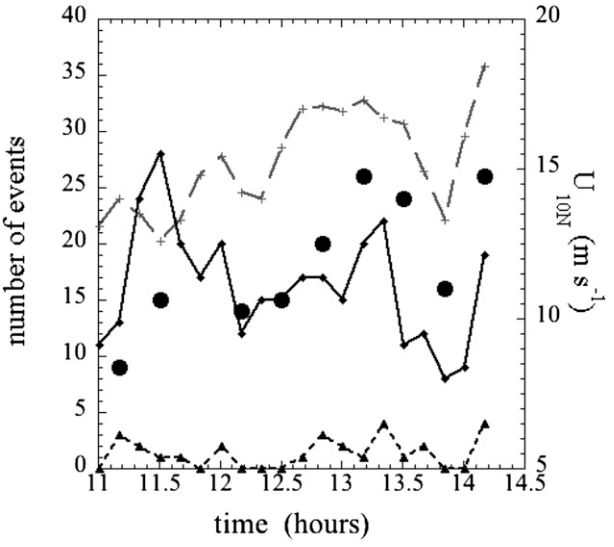

FIG. 19. Number of breaking waves during D313 deployment 4. Shown are the number of breaking waves in each 10-min section of data, as determined from the temporal slope with a threshold of 30° (black dashed lines with triangles) and 17° (black line with diamonds). Mean wind speed is also shown (gray line with crosses) along with estimates of waves breaking from a subset of 10-min video footage segments (black solid circles).

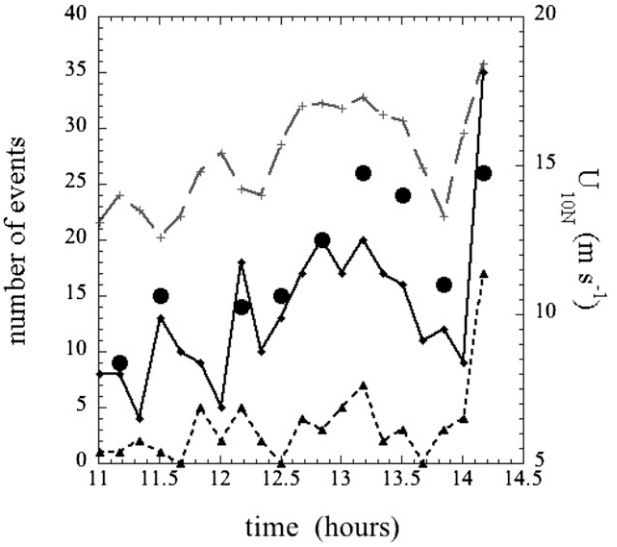

FIG. 20. As in Fig. 19, but using spatial slopes with a threshold of 30° (black dashed lines with triangles) and 24° (black line with diamonds), mean wind speed (gray line with crosses), and video estimates of waves breaking (black solid circles).

Fig. 21 (using the variance of the temporal slope calculated over about 0.2-s segments of the data). As compared to the temporal and spatial slope threshold detection methods (Figs. 19 and 20) it clearly performs better. In this case, closer to 70% of the events detected agree with those seen on the video. We are continuing to refine the method to determine what combinations of surface elevation and slope variance over what time period provides the most robust determination of wave breaking. The outcome of these ongoing investigations will be reported in a future paper.

d. Results from the bubble measurement systems

The acoustic and optical sensors were preset at 2–3-m depths, too deep to detect bubbles in the unexpectedly sheltered locations of the D313 buoy deployments. As a result, a comparison of the bubble data with wave-breaking data from the wave wires was not possible. However, during D320 both acoustic and optical systems successfully measured bubbles. Figure 22 shows an example of the bubble populations measured by the acoustic system along with results from previous studies for comparison. The results are from 1826 UTC on day of D320 at 43°5′N, 17°38′W with a mean wind speed of 14 m s^{-1}, H_s of 2.7 m, and water temperature about 17°C. Figure 23 shows a segment of the time series from one of the fiber-optic sensors as a series of bubbles pass over it. At the start of the sequence, the fiber-optic sensor is initially submerged in the ocean. Then, a passing wave causes the local sea level to dip, exposing the fiber tip to air from time 3.97 to 4.34 s, when the tip is again submerged by the wave. After this a sequence of transients, each indicating the detection of a bubble at the fiber-optic tip, can be seen. These data were obtained on cruise D320 at 1412 UTC on day 173 at 43°42′N, 18°07′W. During this time the wind speed was 7 m s^{-1}, H_s was nearly 2 m and the water temperature was about 17°C. The average depth of the fiber-optic tip is 0.25 m.

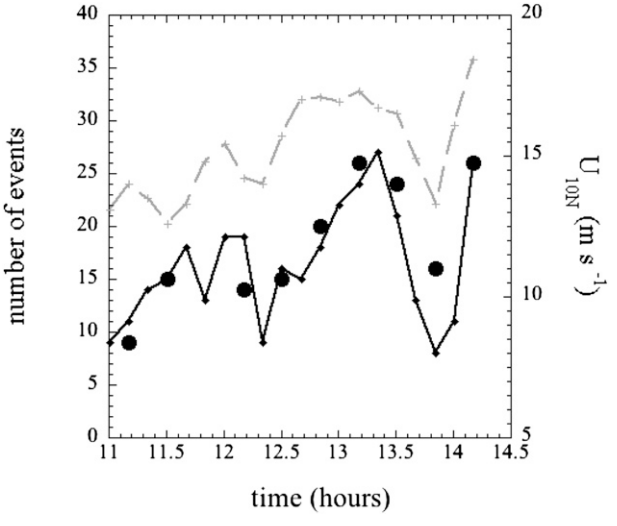

FIG. 21. As in Fig. 20, but showing initial results from a new variance method to determine events (black line with diamonds), mean wind speed (gray line with crosses), and video estimates of waves breaking (black solid circles).

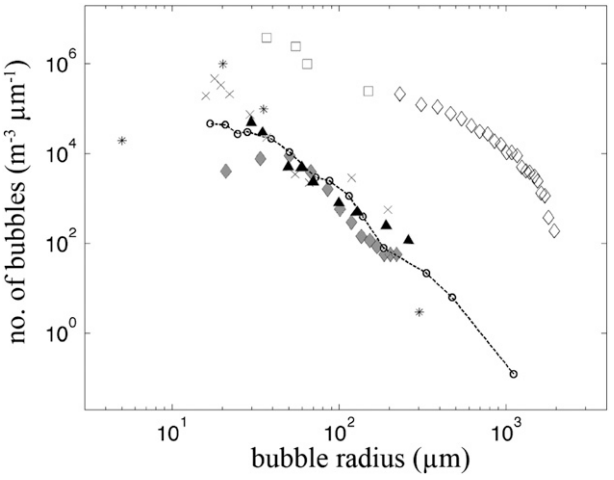

FIG. 22. Bubble-sized spectra from the acoustic system on the spar buoy (black circles) from two hydrophones at mean depths of 0.93 and 2.67 m, over a period of 9 s. For comparison, historic bubble size distributions are shown. Open-ocean measurements include those of Johnson and Cooke (1979; diamonds), Breitz and Medwin (1989; black triangles), Phelps and Leighton (1998; crosses), and Farmer and Vagle (1989; stars). Surf zone measurements are also shown by Deane and Stokes (1999; open diamonds) and Phelps et al. (1997; open squares).

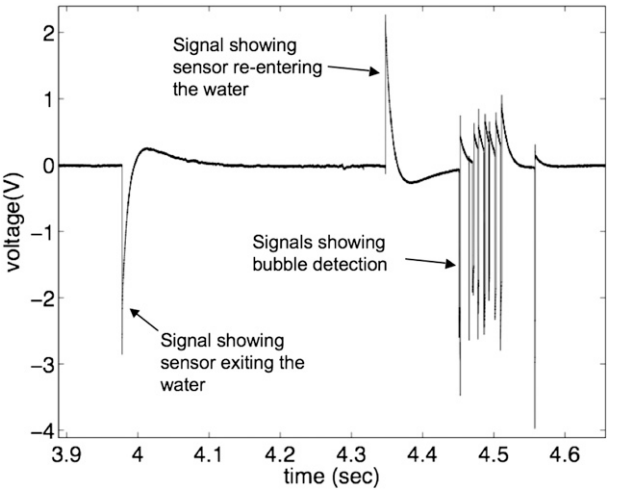

FIG. 23. Time series of output from the optical system showing detection of bubbles.

6. Conclusions

The two deployments (D313 and D320) of the spar buoy have demonstrated that all of the buoy's systems—wave wires, accelerometers, tilt meters, video and still cameras, and acoustic and optical bubble detectors—work in open-ocean conditions; even if not all of the systems have worked simultaneously in each deployment. Although the buoy is large (about 11 m long), it has proven to be possible to deploy and recover it from a research vessel in moderate weather conditions, and it has survived a deployment of 3.5 days in wave conditions with significant waves heights of up to 6 m and peak-to-trough wave heights of up to 9 m. This shows that the buoy is capable of operating autonomously and acquiring the data necessary to achieve the scientific goals for which it was designed and built.

The results from the deployment of the buoy show that the combination of sensors (wave wires and still and video digital cameras) allows the measurement and verification of wave-breaking events in the open ocean. The initial results presented here suggest that the use of either a spatially or temporally based wave slope criterion to detect wave breaking is problematic (the problem with using a temporally based slope criterion was noted by LHS), and further analysis is underway to develop a more robust detection technique for wave breaking based on the wave wire measurements. The advantage that the buoy provides is that the still and video digital camera data allow any proposed detection technique to be verified independently. Once such a detection technique has been verified, much longer buoy deployments can be performed to obtain very extensive wave wire records, and hence more robust statistics on open-ocean wave breaking.

The results from the acoustic and optical systems show the potential to link the wave-breaking detection with the injection of bubble clouds into the ocean by breaking waves. If a robust link can be found between the two, then this should advance our understanding of the wave-breaking contribution to air–sea gas transfers as mediated by bubbles, which is still an outstanding scientific problem (Wanninkhof et al. 2009).

Acknowledgments. This work was supported by the U.K.'s Natural Environment Research Council [Grants NE/C001826/1, NE/C001869/1, NE/C001834/1, NE/G000115/1, NE/G003696/1, and Oceans 2025]. We would also like to acknowledge the officers and crew of the RRS *Discovery* for their help during the deployments of the buoy.

REFERENCES

Bacon, S., and D. J. T. Carter, 1991: Wave climate changes in the North Atlantic and North Sea. *Int. J. Climatol.,* **11,** 545–558.

Banner, M. L., and D. H. Peregrine, 1993: Wave breaking in deep water. *Annu. Rev. Fluid Mech.,* **25,** 373–397.

Blenkinsopp, C. E., and J. R. Chaplin, 2007: Void fraction measurements in breaking waves. *Proc. Roy. Soc. London,* **463A,** 3151–3170.

Breitz, N. D., and H. Medwin, 1989: Instrumentation for in-situ acoustical measurements of bubble spectra under breaking waves. *J. Acoust. Soc. Amer.,* **86,** 739–743.

Brooks, I. M., and Coauthors, 2009: Physical exchanges at the air–sea interface: UK-SOLAS field measurements. *Bull. Amer. Meteor. Soc.,* **90,** 629–644.

Cartellier, A., 2001: Optical probes for multiphase flow characterization: Some recent improvements. *Chem. Eng. Technol.,* **24,** 535–538.

——, and J. L. Achard, 1991: Local phase detection probes in fluid/fluid two-phase flows. *Rev. Sci. Instrum.,* **62,** 279–303.

Deane, G. B., and M. D. Stokes, 1999: Air entrainment processes and bubble size distributions in the surf zone. *J. Phys. Oceanogr.,* **29,** 1393–1403.

Farmer, D. M., and S. Vagle, 1989: Waveguide propagation of ambient sound in the ocean-surface bubble layer. *J. Acoust. Soc. Amer.,* **86,** 1897–1908.

Forristall, G. Z., 2000: Wave crests distribution: Observations and second-order theory. *J. Phys. Oceanogr.,* **30,** 1931–1943.

Gates, J. C., 2004: Measurement of the local optical phase and amplitude in photonic devices using scanning near-field microscopy. Ph.D. thesis, University of Southampton, 177 pp.

Gemmrich, J. R., and D. M. Farmer, 1999: Observations of the scale and occurrence of breaking surface waves. *J. Phys. Oceanogr.,* **29,** 2595–2606.

——, M. L. Banner, and C. Garrett, 2008: Spectrally resolved energy dissipation rate and momentum flux of breaking waves. *J. Phys. Oceanogr.,* **38,** 1296–1312.

Graber, H. C., E. A. Terray, M. A. Donelan, W. M. Drennan, J. C. Van Leer, and D. B. Peters, 2000: ASIS—A new Air–Sea Interaction Spar buoy: Design and performance at sea. *J. Atmos. Oceanic Technol.,* **17,** 708–720.

Holliday, N. P., M. J. Yelland, R. Pascal, V. R. Swail, P. K. Taylor, C. R. Griffiths, and E. Kent, 2006: Were extreme waves in the Rockall Trough the largest ever recorded? *Geophys. Res. Lett.,* **33,** L05613, doi:10.1029/2005GL025238.

Holthuijsen, L. H., and T. H. C. Herbers, 1986: Statistics of breaking waves observed as whitecaps in the open sea. *J. Phys. Oceanogr.,* **16,** 290–297.

Johnson, B. D., and R. C. Cooke, 1979: Bubble populations and spectra in coastal waters: A photographic approach. *J. Geophys. Res.,* **84,** 3761–3766.

Killen, J. M., 1952: A capacitive wave profile recorder. University of Minnesota, St. Anthony Falls Hydraulic Laboratory, Tech. Paper 11, Series B, 7 pp.

Leighton, T. G., S. D. Meers, and P. R. White, 2004: Propagation through non-linear time dependent bubble clouds and the estimation of bubble populations from measured acoustic characteristics. *Proc. Roy. Soc. London,* **460A,** 2521–2550.

Longuet-Higgins, M. S., and M. J. H. Fox, 1978: Theory of the almost-highest wave: Part 2. Matching and analytic extension. *J. Fluid Mech.,* **85,** 769–786.

——, and N. D. Smith, 1983: Measurements of breaking by a surface jump meter. *J. Geophys. Res.,* **88,** 9823–9831.

Manasseh, R., A. V. Babanin, C. Forbes, K. Rickards, I. Bobevski, and A. Ooi, 2006: Passive acoustic determination of wave-breaking events and their severity across the spectrum. *J. Atmos. Oceanic Technol.,* **23,** 599–618.

Melville, W. K., 1996: The role of surface-wave breaking in air-sea interaction. *Annu. Rev. Fluid Mech.,* **28,** 279–321.

——, and P. Matusov, 2002: Distribution of breaking waves at the ocean surface. *Nature,* **417,** 58–63.

Nelson, C. V., 1989: An easily deployed, low cost and light-weight spar buoy for making high frequency wave height measurements. *Proc. OCEANS '89,* Vol. 5, Seattle, WA, IEEE, 1421–1423.

Pedreros, R., G. Dardier, H. Dupuis, H. C. Graber, W. M. Drennan, A. Weill, C. Gue'rin, and P. Nacass, 2003: Momentum and heat fluxes via the eddy correlation method on the R/V L'Atalante and an ASIS buoy. *J. Geophys. Res.,* **108,** 3339, doi:10.1029/2002JC001449.

Phelps, A. D., and T. G. Leighton, 1998: Oceanic bubble population measurements using a buoy deployed combination frequency technique. *IEEE J. Oceanic Eng.,* **23,** 400–410.

——, D. G. Ramble, and T. G. Leighton, 1997: The use of a combination frequency technique to measure the surf zone bubble population. *J. Acoust. Soc. Amer.,* **101,** 1981–1989.

Pitt, E. G., 1991: A new empirically-based correction procedure for ship-borne wave recorder data. *Appl. Ocean Res.,* **13,** 162–174.

Trevorrow, M. V., 2003: Measurements of near-surface bubble plumes in the open ocean with implications for high-frequency sonar performance. *J. Acoust. Soc. Amer.,* **114,** 2672–2684.

Tucker, M. J., 1956: A ship-borne wave recorder. *Trans. Roy. Inst. Nav. Archit.,* **98,** 236–250.

Wanninkhof, R., W. E. Asher, D. T. Ho, C. Sweeney, and W. R. McGillis, 2009: Advances in quantifying air-sea gas exchange and environmental forcing. *Ann. Rev. Mar. Sci.,* **1,** 213–244.

Yelland, M. J., B. I. Moat, R. W. Pascal, and D. I. Berry, 2002: CFD model estimates of the airflow over research ships and the impact on momentum flux measurements. *J. Atmos. Oceanic Technol.,* **19,** 1477–1499.

——, R. W. Pascal, P. K. Taylor, and B. I. Moat, 2009: AutoFlux: An autonomous system for the direct measurement of the air-sea fluxes of CO_2, heat and momentum. *J. Oper. Oceanogr.,* **2,** 15–23.